ACS APPLIED MATERIALS & INTERFACES

www.acsami.org

Research Article

Heteromolecular Bilayers on a Weakly Interacting Substrate: Physisorptive Bonding and Molecular Distortions of Copper–Hexadecafluorophthalocyanine

Qi Wang, Antoni Franco-Cañellas, Jiacheng Yang, Julian Hausch, Samuel Struzek, Mengting Chen, Pardeep Kumar Thakur, Alexander Gerlach,* Steffen Duhm,* and Frank Schreiber*

Cite This: *ACS Appl. Mater. Interfaces* 2020, 12, 14542–14551

Read Online

ACCESS | Metrics & More | Article Recommendations | Supporting Information

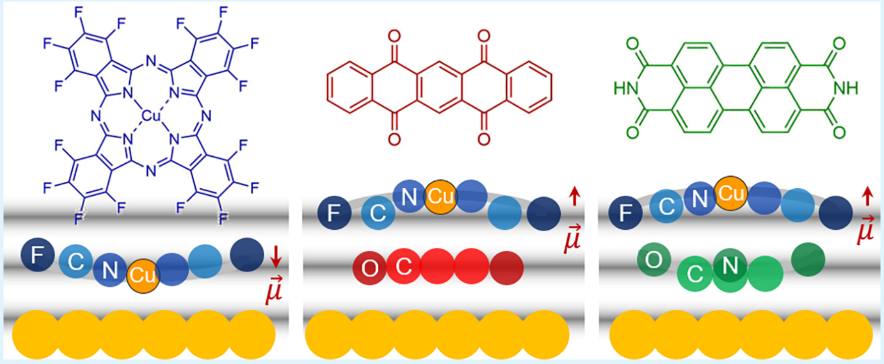

ABSTRACT: Heteromolecular bilayers of π-conjugated organic molecules on metals, considered as model systems for more complex thin film heterostructures, are investigated with respect to their structural and electronic properties. By exploring the influence of the organic–metal interaction strength in bilayer systems, we determine the molecular arrangement in the physisorptive regime for copper–hexadecafluorophthalocyanine ($F_{16}CuPc$) on Au(111) with intermediate layers of 5,7,12,14-pentacenetetrone and perylene-3,4,9,10-tetracarboxylic diimide. Using the X-ray standing wave technique to distinguish the different molecular layers, we show that these two bilayers are ordered following their deposition sequence. Surprisingly, $F_{16}CuPc$ as the second layer within the heterostructures exhibits an inverted intramolecular distortion compared to its monolayer structure.

KEYWORDS: *bilayer structure, adsorption behavior, physisorption, molecular dipole moment, photoelectron spectroscopy, X-ray standing wave measurements*

1. INTRODUCTION

In recent years, heteromolecular structures have attracted a significant amount of attention,[1−4] especially because of their widespread potential for and use in organic (opto)electronic devices. In this context, both the electronic and structural properties of the organic layers are highly relevant as they have a strong impact on the charge carrier transport and thus overall device performance.[5,6] The energy-level alignment at the organic–organic and organic–inorganic interface,[7,8] which is a key issue also for molecular heterostructures, has been the subject of intense research.[9−12] For a better understanding of more elaborate thin film architectures, different bicomponent model systems on single-crystal surfaces have been investigated. Deposited either as molecular mixtures[13−17] or bilayer structures,[18−20] these systems show that the interplay of molecule–molecule and molecule–substrate interactions is rather complex and may even induce unexpected rearrangement processes such as the exchange of the first and the second layer. Importantly, one might also observe significant molecular distortions in those heterostructures,[18,19] which reflect the impact of the different interaction mechanisms on the adsorbed molecules.

To address the fundamental questions raised by these observations, one has to employ different molecule–substrate combinations. Detailed investigations of those systems using complementary experimental techniques allow for a controlled preparation of bilayer structures. It has been observed for heterostructures on Ag(111) that deposition of a second molecular species may induce a complete replacement of weakly interacting molecules in the first layer.[18,19] Generally,

Received: December 17, 2019
Accepted: February 28, 2020
Published: February 28, 2020

https://dx.doi.org/10.1021/acsami.9b22812

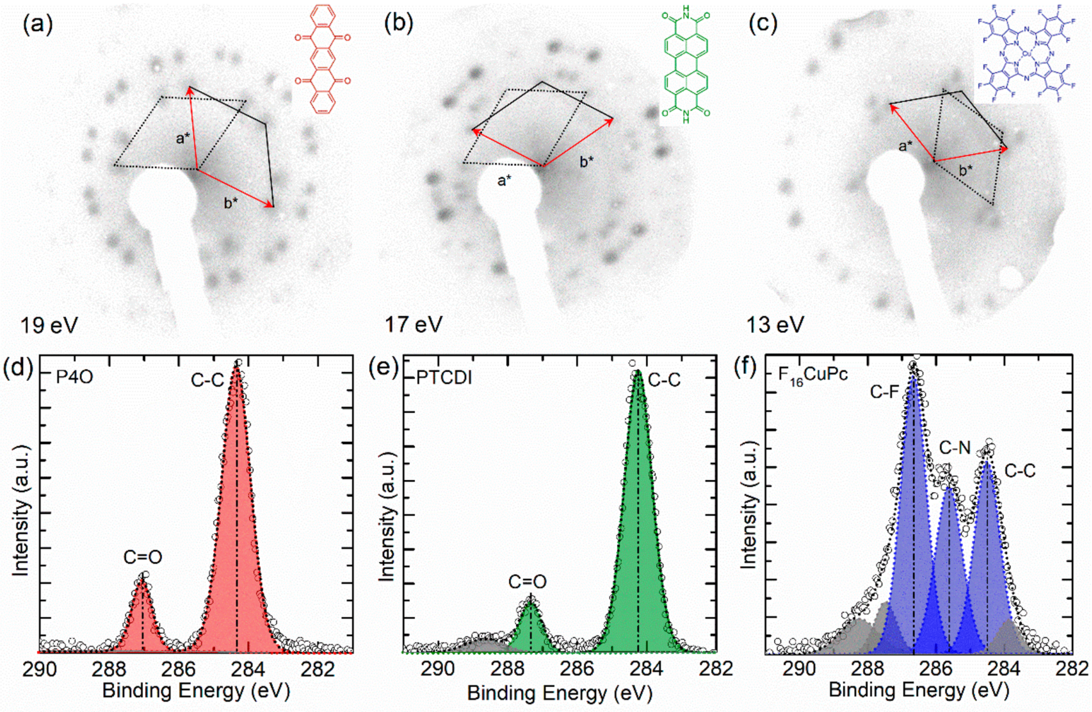

Figure 1. LEED patterns (electron energies included) for 1 monolayer (~4 Å): (a) P4O, (b) PTCDI, and (c) $F_{16}CuPc$ on Au(111), respectively. The unit cell is superimposed in each LEED pattern, whereas the one with red arrows separates two different unit cells in one pattern. HR-XPS measurements of C 1s core-level spectra of (sub)monolayer P4O (d), PTCDI (e), and $F_{16}CuPc$ (f).

chemisorption at organic−metal interfaces can lead to adsorption-induced molecular distortions in the contact layer[21,22] and, consequently, to additional intramolecular dipole moments.[23,24] In contrast, the interaction of molecular monolayers with inert surfaces is dominated by weak dispersion forces.[25−28] To minimize the organic−metal interaction strength, we chose the Au(111) surface. This will allow us to investigate whether such distortions occur in molecular bilayers on weakly interacting substrates as well and whether they are induced by the substrate or rather by intermolecular interactions. Because fluorination of organic semiconductors is expected to further weaken this interaction,[29,30] we employed the electron acceptor copper−hexadecafluorophthalocyanine ($F_{16}CuPc$)[31,32] as the top layer. The fluorination also leads, furthermore, to large chemical shifts in the C 1s core levels,[33,34] which is beneficial for analyzing X-ray photoelectron spectra of the heterostructures.

For reduction of the charge carrier barriers between the organic active layer and the metal electrode, different intermediate layers may be employed between $F_{16}CuPc$ and gold. Accordingly, we use 5,7,12,14-pentacenetetrone (P4O) and perylene-3,4,9,10-tetracarboxylic diimide (PTCDI) (chemical structures inserted in Figure 1) as the insertion layer. Both molecules form well-defined monolayers on clean metal surfaces[35−39] and are chosen because of their rather different surface unit cells,[25,40,41] which allows us to study the possible impact of (in)commensurability on the bilayer growth. For comparison, $F_{16}CuPc$ has also been grown on Au(111) directly and with a P4O or PTCDI layer below. In our present work, the core-level signals and the molecular surface structures, including vertical and planar information, of the mono- and bilayer systems have been studied by high-resolution X-ray photoelectron spectroscopy (HR-XPS), normal-incidence X-ray standing wave (NIXSW) measurements, and low-energy electron diffraction (LEED). In addition, a possible impact of molecular distortions on interface energetics has been measured by ultraviolet photoelectron spectroscopy (UPS).

2. EXPERIMENTAL METHODS

The HR-XPS and NIXSW experiments were performed at beamline I09 at Diamond Light Source (DLS, UK) using the available soft (110−1100 eV) and hard (2.1−18 keV) X-ray beams.[42−44] Sample preparation and measurements were performed in situ under ultra-high-vacuum conditions. The analysis chamber (base pressure: 3×10^{-10} mbar) contains a VG Scienta EW4000 HAXPES hemispherical photoelectron analyzer, which is mounted at 90° relative to the incident X-ray beam. The reflectivity and photoelectron core-level spectra of all elements were recorded at different photon energies E (42 data sets) within a ±4.5 eV interval around the Bragg energy E_{Bragg} (~2.63 keV) of Au(111). The photoelectron yield Y_{P} ($E - E_{\mathrm{Bragg}}$) and the reflectivity were modeled, taking into account the experimental geometry and the nondipole corrections associated with it.[29] The gold substrate was cleaned by several cycles of Ar^{+} ion bombardment and annealing (400−500 °C). The π-conjugated organic molecules (COMs) were sublimated onto the single-crystal surface (held at room temperature) by physical vapor deposition from home-built, resistively heated cells with deposition rates of about ~0.2 Å/min. The nominal film mass thickness was monitored by a quartz-crystal microbalance positioned near the sample.

Low-energy electron diffraction (LEED) was performed using a Micro-Channel-Plate LEED (OCI BDL800IR-MCP), which is installed in the analysis chamber at I09. The LEED patterns were recorded using typical energies $E_{\mathrm{kin}} < 20$ eV. LEED pattern simulations were done using the LEEDpat[45] software.

Thickness-dependent ultraviolet photoelectron spectroscopy (UPS) and XPS measurements were carried out at Soochow University in an ultra-high-vacuum system consisting of three interconnected chambers: an evaporation chamber (base pressure: 3×10^{-10} mbar), an annealing and sputtering chamber (3×10^{-10}

mbar), and an analysis chamber (base pressure: 2 × 10^{-10} mbar).[28] UPS experiments were performed using monochromatized He I radiation (21.22 eV) and a Specs PHOIBOS 150 analyzer. The energy resolution was set to 80 meV. The angle between the incident beam and the sample was fixed to 40°. The spectra were collected at photoelectron takeoff angles (θ) of 45° with an acceptance angle of ±12° along the $\Gamma-M$ direction of Au(111). A sketch of the measurement geometry can be found in ref 28. The secondary electron cutoff (to determine the vacuum level) was measured in normal emission with a bias potential of −3 V. XPS was performed using a monochromatized Al Kα source (1486.6 eV). The data analysis was carried out by a nonlinear least-squares fitting routine, using Gaussian/Lorentzian peak shapes and a Shirley background. The error bar for the binding energies (BE) in UPS is estimated to be ±0.05 eV. All measurements have been performed at room temperature (295 K).

3. EXPERIMENTAL RESULTS

3.1. Homomolecular Systems. We start discussing the in-plane structure of P4O, PTCDI, and F_{16}CuPc monolayers on Au(111), as determined by LEED (Figure 1a−c). The measurements show pronounced diffraction patterns stemming from the adsorbates. The three surface unit cells (parameters in Table S1, Supporting Information) are hexagonal and in good agreement with previous studies.[18,46,47] From these, we can conclude that molecules are essentially lying down on the surface. Additional simulation results of LEED patterns can be found in Figure S1.

The chemical analysis by HR-XPS is shown in Figure 1d. The two peaks in the C core-level spectrum of P4O on Au(111) are labeled as C−C (284.34 eV) and C=O (287.05 eV), as in previously reported results.[35] Similarly, the C 1s spectrum of the PTCDI (Figure 1e) monolayer allows one to distinguish two peaks, defined as C−C (perylene core) located at the BE of 284.24 eV and C=O (functional group) at a BE of 287.35 eV, with a small shake-up satellite located at higher BE. In the case of F_{16}CuPc, the C 1s core-level shows three distinct peaks, which appear at binding energies of 284.50, 285.62, and 286.66 eV and are assigned to carbon atoms bound to carbon (C−C), nitrogen (C−N), and fluorine (C−F) atoms, respectively.[29,48,49] The peak located at the lowest BE (283.89 eV) is attributed to a small portion of carbon atoms bound to the substrate (C−Au) because of broken C−F bonds,[34,44] whereas the shoulder (two gray peaks) at higher BE corresponds to shake-up satellites.[18,50] The relative chemical shifts of all three peaks correspond to F_{16}CuPc in multilayers on polycrystalline Au,[49] which indicates physisorption of F_{16}CuPc on the Au(111) surface. The assignment is done following the molecular stoichiometry and is in line with previous studies.[51,52] Importantly, the relative BE positions of the three carbon species can be used as criteria to fit the bilayer core-level spectra.

Having established the spectroscopic features of the core levels and the in-plane structure of the three different monomolecular systems, we now turn to the vertical adsorption geometry and present the corresponding XSW results, which provide precise adsorption distances (typical precision <0.05 Å[54]). The analysis of the photoelectron yield Y_P (see Supporting Information) in the standing wave field, which is generated by the interference of incident and Bragg-diffracted X-ray standing waves, gives the coherent position (P_H) and coherent fraction (f_H). P_H can be used to determine the average vertical adsorption distance (d_H) of the different adsorbate atoms by $d_H = (P_H + n)d_0$,[55] with $d_0 = 2.35$ Å being the lattice plane spacing of gold along the [111] direction and n being an integer number[55] that arises from the periodicity of the standing wave field, which is important to distinguish between the molecules adsorbing in the first layer and those in the second. f_H is a parameter describing the degree of vertical order of the respective adsorbate atoms.[18] Because of the surface relaxation of Au and to obtain ideal adsorption distances, we corrected the values as stated in ref 53.

The complete XSW data analysis of the homomolecular systems P4O, PTCDI, and F_{16}CuPc on Au(111), which is based on the HR-XPS fitting model discussed in Figure 1, is displayed in Figure S2, Figure S3, and Figure S4. As shown in Figure S2, also the adsorption distance of the oxygen atoms in P4O have been measured using the (222) Bragg reflection of gold (photon-energy range 5266 ± 4.5 eV) to avoid the overlapping gold Auger peak,[25] which is encountered for the (111) reflection. The downside of using the higher order reflections is that fewer photoelectrons are generated, thus leading to weaker and noisier signals. To account for this, we associated a larger error of ~0.1 Å with the adsorption distances. By applying the equation for P_H, we determine the adsorption distance as $d_H = 3.17$ Å.[55] When using the (111) Bragg reflection of Au (2.63 keV), it is only possible to measure the adsorption distance of carbon atoms in P4O, for which we distinguish two carbon species, one bound to another carbon atom (3.34 Å) and the one bound to an oxygen atom (3.38 Å). In Figure 2, the adsorption geometry, including d_H, of the three molecules on Au(111) is shown. Because of the high-quality XSW data and the core-level fitting model employed, the adsorption distance of different inequivalent species within the same core-level signal is accessible (full list of adsorption distances in Table 1). Monolayers of P4O and PTCDI on the surface remain in a flat-lying configuration with d_H of 3.35 and 3.33 Å, that is, in line with previous studies with only minor differences in PTCDI.[25,35] A similar agreement with the literature is found for F_{16}CuPc, which absorbs flat on the surface with an average adsorption distance of 3.35 Å, similar to the results reported by de Oteyza et al.[33] Thanks to

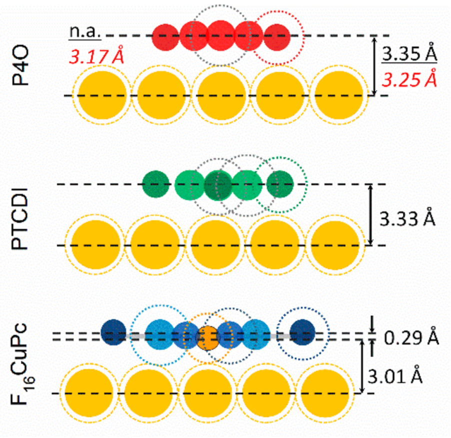

Figure 2. Sketch of the vertical adsorption geometries of P4O, PTCDI, and F_{16}CuPc on Au(111) (in Å) as inferred from the XSW measurements (Figure S2, Figure S3, Figure S4, and Table 1). Note that for P4O/Au(111) the black numbers correspond to E_{Bragg} = 2.635 keV and the red numbers to E_{Bragg} = 5.266 keV. Elements with dashed lines are drawn according to their van der Waals radii. The displayed adsorption distances were calculated by taking into account the surface reconstruction observed on the gold surfaces.[53]

Table 1. Adsorption Distance of P4O, PTCDI, and $F_{16}CuPc$ on Au(111) in Å as Derived from XSW Measurements According to the Relation $d_H = (P_H + n)d_0$[a]

	Å								
	C−C	C−N	C−F	C=O	C_{av}	F	N	Cu	O
P4O (2.63 keV)	3.34	*	*	3.38	3.35	*	*	*	–
P4O (5.26 keV)	3.26	*	*	–	3.25	*	*	*	3.17
PTCDI	3.33	*	*	3.33	3.33	*	3.34	*	–
$F_{16}CuPc$	3.16	3.05	3.34	*	3.20	3.30	3.12	3.01	*

[a]* means that the element is not present in the molecule and (−) that the results could not be obtained or decoupled in the analysis. The final adsorption distances were calculated by taking into account the surface reconstruction occurring for this substrate.[53] The different carbon species are labeled "C−C", "C−N", "C−F", and "C=O", whereas "C_{av}" gives the averaged adsorption distance of all carbon atoms within one molecule.

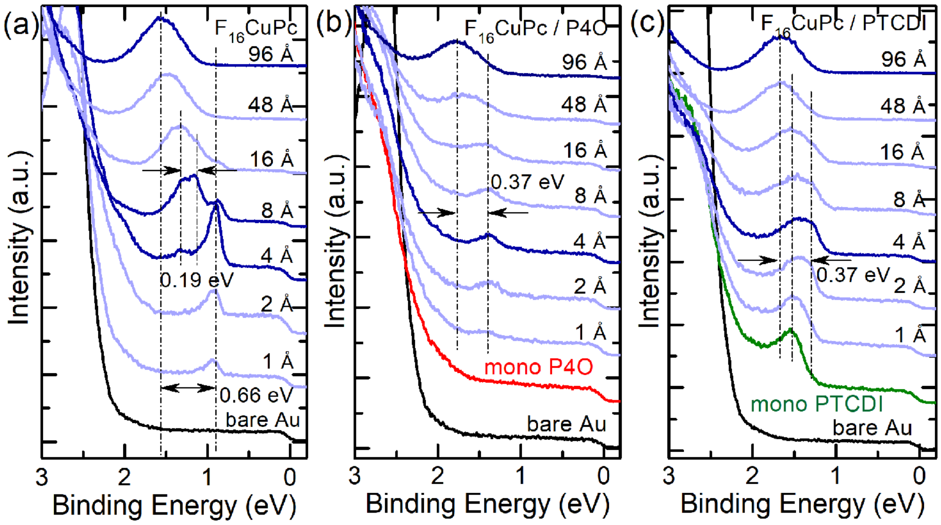

Figure 3. UPS spectra taken at 45° for the stepwise-deposited COMs on Au(111). (a) Pure $F_{16}CuPc$ grown on Au(111) with the mono- and multilayer spectra highlighted by darker lines. UPS spectra of $F_{16}CuPc$ deposited on a monolayer of P4O/Au(111) (b) and PTCDI/Au(111) (c). For the heterostructures the nominal monolayer (4 Å) and multilayer (96 Å) thickness of $F_{16}CuPc$ spectra are indicated. Vertical lines refer to the position of the HOMO. Survey spectra (up to 14 eV BE) of these systems can be found in Figure S5.

the improved setup at I09 and the state-of-the-art photoelectron spectrometer, we have been able to resolve, in contrast to the previous report, different inequivalent carbon species and nitrogen. Thus, as shown in Figure 2, the central copper ion takes the lowest height (3.01 Å) compared to the other elements,[29] that is, similar to other metal−phthalocyanine molecules.[24,56−58] Influenced by the copper atom, the nitrogen atoms that are bound to it show an intermediate height (3.12 Å) with respect to the Cu and F atoms. Moreover, carbon atoms in different chemical environments show a similar trend; that is, the carbon atoms in C−F bonds have the largest adsorption distance (3.34 Å), whereas carbon in C−N bonds are closer to nitrogen itself. Comparing all elements in $F_{16}CuPc$, we conclude that $F_{16}CuPc$, which is planar in the gas phase,[59,60] shows a significant distortion on Au(111) as the central Cu atom is located below and F atoms above the average adsorption distance, which was observed for the same molecules on Ag(111) and Cu(111).[29]

3.2. Heteromolecular Systems. Having a detailed picture of the three monomolecular systems on Au(111), including their in-plane and vertical geometry as well as their electronic properties, we now proceed to the heteromolecular bilayer structures. For the heterostructures, $F_{16}CuPc$ was vacuum-sublimed on monolayers of P4O and PTCDI. For the UPS and XPS measurements, the nominal thickness of the template layer has been as close to monolayer coverage as possible while making sure that it does not exceed one monolayer; for LEED, HR-XPS, and XSW measurements these monolayers have been prepared by thermal desorption of multilayers.

Prior to discussing the coverage-dependent evolution of the valence-electron region spectra of the bilayers, we show the UPS spectra of $F_{16}CuPc$ in Figure 3a. With the deposition of $F_{16}CuPc$, the intensity of the substrate-derived Fermi edge is attenuated and characteristic peaks of $F_{16}CuPc$ appear: the highest occupied molecular orbital (HOMO)-derived peak centered at 0.90 eV (for submonolayer and monolayer thickness). The intensity of this peak becomes strongest at the nominal monolayer coverage (4 Å), and increasing the coverage leads to an attenuation of this feature because of the limited probing depth of UPS. For an $F_{16}CuPc$ monolayer thickness, a new feature appears at higher BE (~1.31 eV) close to the monolayer HOMO peak, which apparently splits into two peaks. The fine structure of the splitting, which can be observed only for a thickness corresponding to a monolayer (4 Å) and bilayer (8 Å), could be explained by considering the formation of dimers, a phenomenon that has been observed for PbPc on HOPG as well.[58] Further experiments will be required to verify this hypothesis in general.

Figure 3b,c shows the coverage-dependent evolution of UPS spectra of $F_{16}CuPc$ deposited on Au(111) precovered by the two adlayers (P4O and PTCDI). For the $F_{16}CuPc$/P4O bilayer (Figure 3b), that is, with a P4O monolayer on Au, because of the gold d-band at a low binding energy (~2 eV), the HOMO peak of P4O is disturbed by the Au features. The

https://dx.doi.org/10.1021/acsami.9b22812
ACS Appl. Mater. Interfaces 2020, 12, 14542−14551

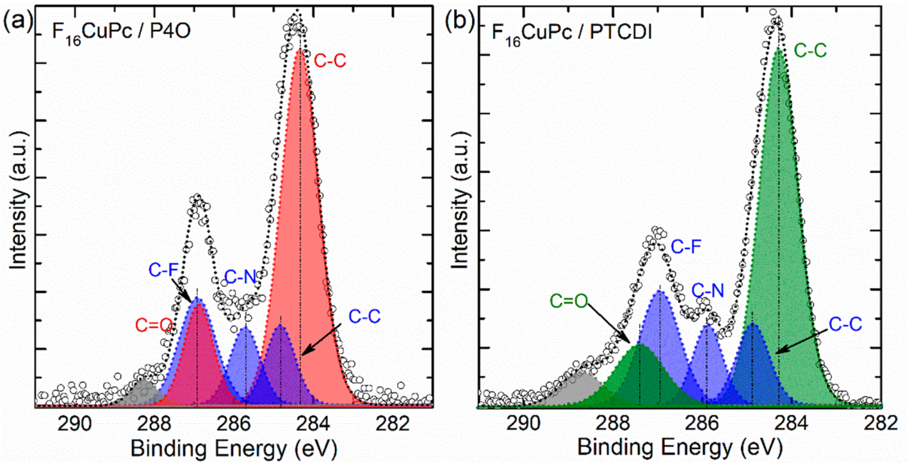

Figure 4. HR-XPS measurements of C 1s core-level spectra for bilayer systems of $F_{16}CuPc/P4O$ (a) and $F_{16}CuPc/PTCDI$ (b) on Au(111). Spectra are taken with $h\upsilon$ = 800 eV. The monolayers of the template molecule were prepared by desorption, and then the monolayer $F_{16}CuPc$ was deposited on top. The color code is adapted from Figure 1. Red areas belong to P4O, green areas belong to PTCDI, and blue areas indicate the $F_{16}CuPc$ contribution.

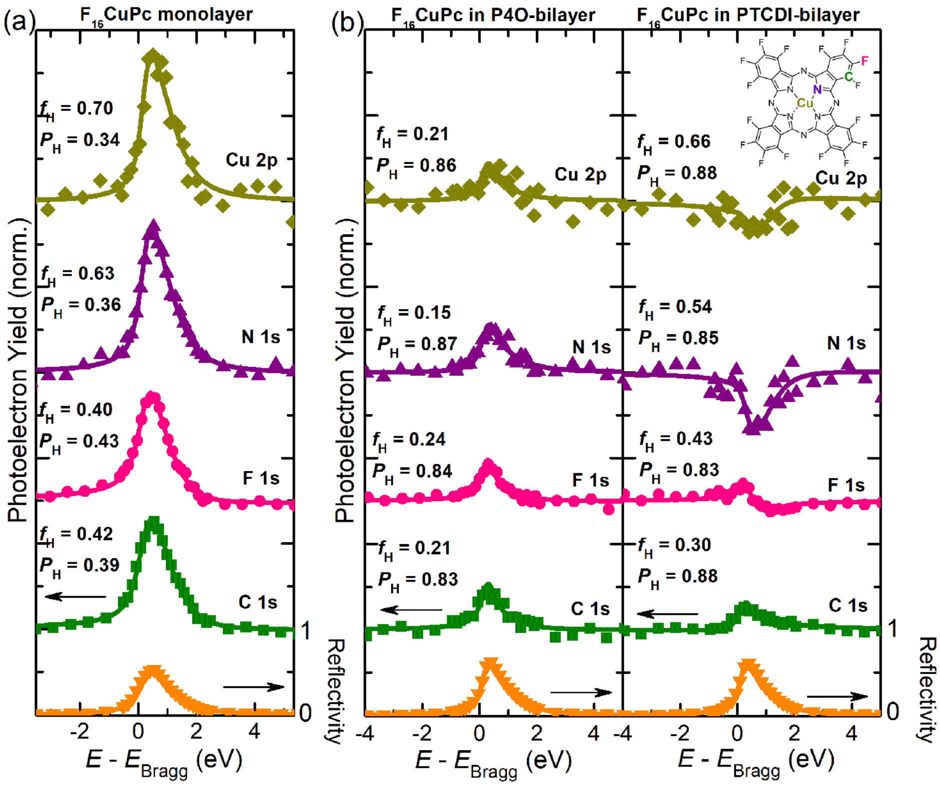

Figure 5. XSW measurements for an $F_{16}CuPc$ (sub)monolayer directly adsorbed on Au(111) (a), on top of a P4O (b), and PTCDI (c) monolayer, both on the same substrate. The inset describes the color code of different components in $F_{16}CuPc$.

HOMO-derived peak of $F_{16}CuPc$, located at a BE of 1.40 eV at one monolayer thickness (4 Å), gradually emerges with increasing coverage. It shifts by 0.37 eV toward higher BE with further $F_{16}CuPc$ deposition as expected because of the reduced photo hole screening by the substrate.[35] This is in line with $F_{16}CuPc$ and P4O forming a bilayer system on Au(111) as the valence band (VB) features of $F_{16}CuPc$ are different from those in Figure 3a, indicating that the molecules are not in contact with the substrate. The HOMO peak shift of $F_{16}CuPc$ is found to be similar for deposition on the PTCDI monolayer. Here, the $F_{16}CuPc$ HOMO peak features become visible, whereas the PTCDI HOMO signal (1.52 eV in green curve) vanishes. Notably, in this bilayer the HOMO position of $F_{16}CuPc$ also shifts by 0.37 eV with further deposition of $F_{16}CuPc$, that is, by the same amount as that for the P4O interlayer on Au(111).

Adapting the fitting model from Figure 1, we analyze the C 1s core levels of (sub)monolayer $F_{16}CuPc$ on Au(111) precovered by a monolayer of P4O (Figure 4a) and PTCDI (Figure 4b). In Figure 4a, the C−C and C═O peaks of P4O (red areas) are visible with a BE difference of 2.54 eV, which is identical to the monolayer spectra of P4O on Au(111) (Figure

Table 2. Adsorption Distance d_H of $F_{16}CuPc/P4O$ and $F_{16}CuPc/PTCDI$ Bilayers on Au(111) Determined by XSW Measurements According to the Relation $d_H = (P_H + n)d_0$

	$F_{16}CuPc/P4O/Au(111)$ (Å)					$F_{16}CuPc/PTCDI/Au(111)$ (Å)			
	C_{av}	F	N	Cu		C_{av}	F	N	Cu
$F_{16}CuPc$	6.51	6.56	6.71	6.67	$F_{16}CuPc$	6.69	6.61	6.67	6.74
P4O	3.38	*	*	*	PTCDI	3.33	*	3.43	*

1a). Meanwhile, the C signals attributed to $F_{16}CuPc$ (blue areas) prevail with similar BE shifts for each species compared to those shown in Figure 1f; that is, the C−N (C−F) component is found at 0.91 eV (2.12 eV) higher BE than C−C. The residual area at ∼288 eV most likely corresponds to a shake-up peak. The results in Figure 4b demonstrate that all components related to PTCDI (green areas) and $F_{16}CuPc$ (blue areas) occur at BE positions, which agree with the monolayer fitting results. Specifically, the two carbon species of PTCDI exhibit a BE difference of 3.11 eV, and the carbon peaks of $F_{16}CuPc$ are distributed as they are in Figure 1f and Figure 4a. For comparison, the XPS core-level spectra of $F_{16}CuPc$ monolayer (∼4 Å) and multilayers (∼96 Å) on the precovered Au(111) are shown in Figure S6.

After the investigation of the chemical properties by XPS, the adsorption distances were measured using the XSW technique. The photoelectron yield Y_P ($E - E_{\mathrm{Bragg}}$) and corresponding fits for $F_{16}CuPc$ in mono- and bilayers together with the corresponding least-squares fits are displayed in Figure 5. Details for all $F_{16}CuPc$ signals have been measured and the corresponding element-specific results are summarized in Table 2. After $F_{16}CuPc$ deposition on the P4O−adlayer, the P4O molecules remain within the error bar at the same height as that before the addition of the second layer, that is, at 3.38 Å (vs 3.34 Å). The Cu and N atoms of $F_{16}CuPc$ are found to be about 3.3 Å above P4O, that is, at similar intermolecular distances as CuPc/P4O[18] on Ag(111). The F and C atoms are found to be slightly closer to the P4O molecules with a difference of 0.11 Å, which indicates a soft bending of the molecule in the second layer.

For the PTCDI-bilayer system, we find that the adsorption geometry of the PTCDI interlayer changes upon deposition of $F_{16}CuPc$. Initially, PTCDI monolayers on Au(111) are essentially planar, that is, with its two carbon species and nitrogen atom at identical adsorption distances. According to the XSW data analysis, we find that the C atoms in PTCDI remain at the adsorption distance of the monolayer system. In contrast, the N atoms are located at an adsorption distance of 3.43 Å, which is 0.10 Å higher than the C atoms. This significant difference between C and N in PTCDI means that the initially flat molecule is bent because of the interaction with $F_{16}CuPc$ molecules in the second layer (see Figure S4 and Table 2). The Cu atoms are found 3.41 Å above the C atoms of PTCDI, whereas the F atoms are only 3.28 Å above, which is similar to the adsorption distance differences of CuPc and PTCDA[61] on Ag(111). Thus, the adsorption geometry of $F_{16}CuPc$ is qualitatively similar to that of the P4O bilayer with a spread of 0.13 Å within the molecule.

As discussed above, $F_{16}CuPc$ shows a slightly distorted structure when adsorbed on Au(111) with the Cu atom located at the lowest and F atoms at the highest position. According to the XSW measurements, it adsorbs with an inverted intramolecular distortion (∼0.1 Å) on top of both intermediate layers, compared to the $F_{16}CuPc$ monolayer on Au ($\Delta d_H = 0.29$ Å). Considering the carbon backbones of both bilayer systems, the distance Δd_H between $F_{16}CuPc$ and the adlayers are 3.13 Å (P4O-bilayer) and 3.36 Å (PTCDI-bilayer). There are differences between the coherent fractions of both systems as well. $F_{16}CuPc$ on PTCDI shows values very similar to the monolayer case, whereas on P4O, the f_H for the different elements is reduced. This could be explained by the different packing of PTCDI and P4O on Au(111), which induces a different degree of disorder in the second layer. Overall, the adsorption geometry of $F_{16}CuPc$ in the bilayers is found to be significantly different compared to the distorted structure of the monolayer on Au(111); that is, in the bilayer $F_{16}CuPc$ molecules show an inverted intramolecular distortion because of the insertion of the first layer.

4. DISCUSSION AND CONCLUSION

$F_{16}CuPc$ Monolayer. The results of the present paper are schematically summarized in Figure 6, including the adsorption geometry, that is, with the element-specific bonding distances of the $F_{16}CuPc$ monolayer and bilayers as they were determined by XSW measurements. In addition, the energy level diagram derived by UPS is displayed at the bottom. By combining these results, we can draw a picture of the $F_{16}CuPc$ monolayer system as it has been discussed. The vacuum level (VL) (for details, see Figure S7 and Figure S8) position with increasing film coverage (Figure 6) provides further insight into the interaction strength for the mono- and hetero-molecular interfaces.[26,28,62] Figure 6a illustrates the distorted adsorption geometry of $F_{16}CuPc$ with the copper atom at the lowest distance and fluorine atoms being 0.29 Å higher. Upon initial deposition of $F_{16}CuPc$, the vacuum level shows a steep decrease (ΔVL = 0.45 eV), which nearly saturates at the monolayer coverage (Figure S7 and Figure S8). This behavior confirms flat-lying molecules in the monolayer and also a multilayer growth regime. The observed VL shifts can be explained to a large extent by Pauli repulsion. However, the distortion of this molecule according to XSW results and the corresponding dipole moment ($\vec{\mu}$) needs to be taken into account for a complete picture of the adsorption behavior and energy levels. In general, vacuum-level shifts ΔVL at organic−metal interfaces can have two contributions:[24,63]

$$\Delta \mathrm{VL} = \Delta\Phi_{\mathrm{dip}} + \Delta\Phi_{\mathrm{bond}}$$

In this equation, $\Delta\Phi_{\mathrm{bond}}$ contains the effect of the molecule−metal interaction, which is mainly caused by Pauli repulsion for the weakly interacting $F_{16}CuPc/Au(111)$. The other contribution $\Delta\Phi_{\mathrm{dip}}$ is proportional to the distortion-induced dipole moment ($\vec{\mu}$)[64] shown in Figure 6a. It is because fluorine atoms with negative partial charge take an adsorption distance, which is 0.29 Å higher than that of copper atoms with their positive partial charge. For $F_{16}CuPc$ monolayers on Au(111), the observed ΔVL can be ascribed to the combination of the molecular dipole moment[24,63] and the pushback effect (with ΔVL increasing for decreasing adsorption distance[65,66]).[67,68]

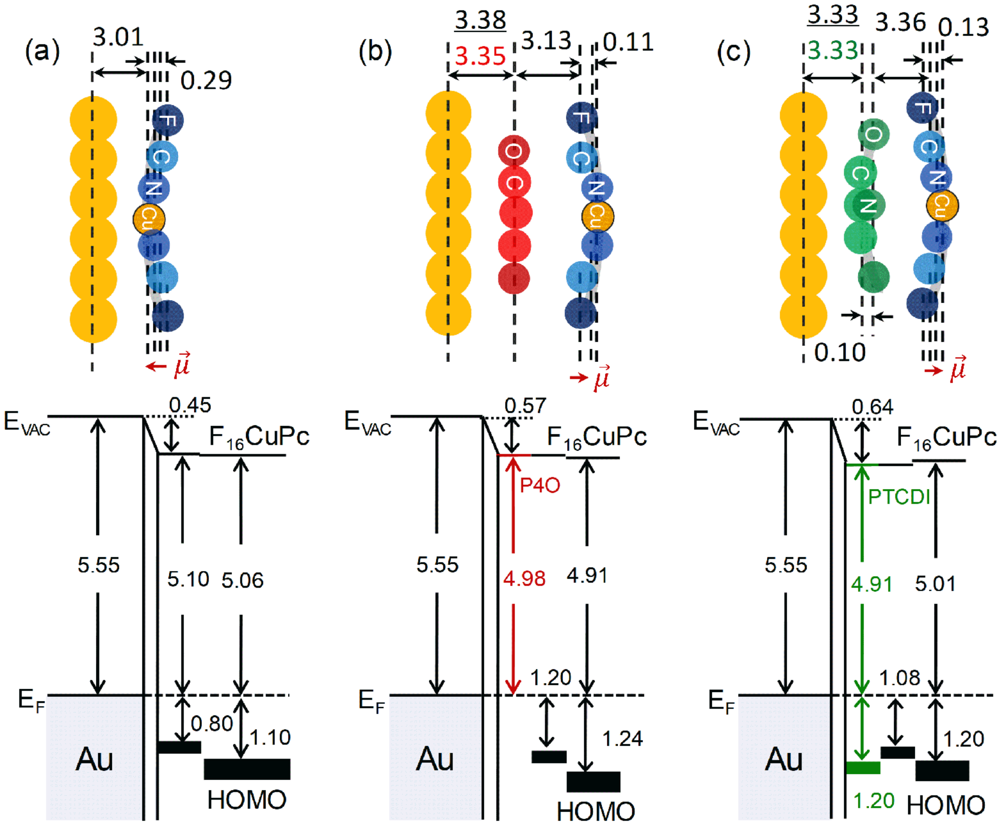

Figure 6. Adsorption geometries F_{16}CuPc (a), F_{16}CuPc/P4O (b), and F_{16}CuPc/PTCDI (c) on Au(111). In Figure 6b,c, black values indicate bilayer systems and red values (bottom) are from the monolayer systems for comparison. Real adsorption distances were calculated considering the surface reconstruction of Au(111).[53] Energy-level diagram of the three interfaces are determined by UPS measurements.

F_{16}CuPc Bilayers. Within the P4O-derived bilayer (Figure 6b), the P4O molecules remain virtually at the same adsorption distance as those in the monolayer system (3.35 Å vs 3.38 Å). More importantly, F_{16}CuPc on P4O adsorbs in the geometry with Cu and N atoms repelled by ~0.11 Å relative to the C and F atoms. This is in contrast to the strong upward bending of F atoms in F_{16}CuPc monolayers on Au(111). It can be speculated that the repulsive interaction of the F atoms with the Au(111) substrate is weakened by the template layer. The lack of interaction between P4O and F_{16}CuPc is further supported by the absence of a notable vacuum-level shift, whereas the slight vacuum-level shift (~0.10 eV) at this interface can be ascribed to the distortion of F_{16}CuPc itself. A similar behavior is found for the PTCDI/F_{16}CuPc bilayer, where the VL is lowered by a monolayer of PTCDI on Au(111) and deposition of F_{16}CuPc on top causes no further VL change at low coverages (only 0.10 eV for thicker films). The XSW results give evidence of the weak coupling between F_{16}CuPc and PTCDI. With F_{16}CuPc deposited to form the bilayer, the planar PTCDI molecule is slightly bent with its nitrogen atoms closer to the F_{16}CuPc molecule, whereas F_{16}CuPc shows more of the inverse bending (0.13 Å), as was found for the P4O-derived bilayer. Apart from that, in both bilayers, differences between the highest adsorbed element in the first layer and the lowest adsorbed element in the second layer (F_{16}CuPc) are similar, that is, 3.13 and 3.18 Å, demonstrating again that P4O and PTCDI have a comparable template function for F_{16}CuPc.

In summary, we have studied the geometric and electronic structure, specifically, the adsorption distances and vacuum-level shifts, at the organic−organic and organic−metal interfaces of F_{16}CuPc, F_{16}CuPc/P4O, and F_{16}CuPc/PTCDI bilayer systems on Au(111). Our measurements have shown that the three molecules are physisorbed on this substrate and that, as expected for weak interactions, the HOMO positions of F_{16}CuPc in the two different bilayer systems are nearly identical. Moreover, the fluorine-upward distorted structure of the F_{16}CuPc monolayer on Au(111) is confirmed by XPS and XSW, together with the support of UPS and LEED. Notably, the advantages of the XSW technique have been used to resolve the adsorption distance of two different layers with an error bar of <0.1 Å, demonstrating the potential of further investigations on such heterostructures. Therefore, the growth of F_{16}CuPc as the second layer is confirmed by XSW and UPS measurements. For the P4O-derived bilayer, the P4O molecules as the bottom layer representing the contact with the substrate remain essentially at the same bonding distances as P4O in monolayers on Au. Deviations, however, occur for the F_{16}CuPc molecules in the second layer with an intramolecular downward distortion. The XSW results reveal that, in the F_{16}CuPc/PTCDI bilayer, both molecules show different adsorption behaviors compared to those in the monolayers. In this bilayer system, there is the upward bending of nitrogen in PTCDI and downward bending of fluorine in F_{16}CuPc, which indicates an attraction between these two materials. An intramolecular distortion of F_{16}CuPc is found for these bilayers, yet with inverted direction compared to the adsorption on metal substrates. Overall, we have shown that also in the physisorptive regime the substrate plays a crucial role in the conformation of adsorbates.

■ ASSOCIATED CONTENT

Supporting Information

The Supporting Information is available free of charge at https://pubs.acs.org/doi/10.1021/acsami.9b22812.

> Simulation of LEED patterns, Y_P data of the oxygen signal of P4O determined at the (222) Bragg energy of Au, real-time XPS during the annealing of F_{16}CuPc multilayer, XSW results of monomolecular systems, additional UPS results, thickness-dependent XPS measurements, secondary-electron cutoff and coverage-dependent evolution of the vacuum level shift, and N 1s core levels of corresponding systems (PDF)

■ AUTHOR INFORMATION

Corresponding Authors

Alexander Gerlach − *Institut für Angewandte Physik, Universität Tübingen, 72076 Tübingen, Germany;* orcid.org/0000-0003-1787-1868; Email: alexander.gerlach@uni-tuebingen.de

Steffen Duhm − *Institute of Functional Nano & Soft Materials (FUNSOM), Jiangsu Key Laboratory for Carbon-Based Functional Materials & Devices and Joint International Research Laboratory of Carbon-Based Functional Materials and Devices, Soochow University, Suzhou 215123, People's Republic of China;* orcid.org/0000-0002-5099-5929; Email: duhm@suda.edu.cn

Frank Schreiber − *Institut für Angewandte Physik, Universität Tübingen, 72076 Tübingen, Germany;* orcid.org/0000-0003-3659-6718; Email: frank.schreiber@uni-tuebingen.de

Authors

Qi Wang − *Institut für Angewandte Physik, Universität Tübingen, 72076 Tübingen, Germany;* orcid.org/0000-0002-9777-3637

Antoni Franco-Cañellas − *Institut für Angewandte Physik, Universität Tübingen, 72076 Tübingen, Germany;* orcid.org/0000-0001-7767-9611

Jiacheng Yang − *Institute of Functional Nano & Soft Materials (FUNSOM), Jiangsu Key Laboratory for Carbon-Based Functional Materials & Devices and Joint International Research Laboratory of Carbon-Based Functional Materials and Devices, Soochow University, Suzhou 215123, People's Republic of China*

Julian Hausch − *Institut für Angewandte Physik, Universität Tübingen, 72076 Tübingen, Germany*

Samuel Struzek − *Institut für Angewandte Physik, Universität Tübingen, 72076 Tübingen, Germany*

Mengting Chen − *Institute of Functional Nano & Soft Materials (FUNSOM), Jiangsu Key Laboratory for Carbon-Based Functional Materials & Devices and Joint International Research Laboratory of Carbon-Based Functional Materials and Devices, Soochow University, Suzhou 215123, People's Republic of China*

Pardeep Kumar Thakur − *Diamond Light Source, Oxfordshire OX11 0DE, United Kingdom;* orcid.org/0000-0002-9599-0531

Complete contact information is available at: https://pubs.acs.org/10.1021/acsami.9b22812

Notes

The authors declare no competing financial interest.

■ ACKNOWLEDGMENTS

The authors thank the Diamond Light Source for access to beamline I09, and its staff for excellent support during the beamtime. Financial support from the Soochow University−Western University Center for Synchrotron Radiation Research, the Collaborative Innovation Center of Suzhou Nano Science & Technology (NANO−CIC), and the Deutsche Forschungsgemeinschaft (DFG) is gratefully acknowledged. Q.W. gratefully acknowledges financial support from the China Scholarship Council.

■ REFERENCES

(1) Akaike, K.; Onishi, A.; Wakayama, Y.; Kanai, K. Structural Disordering Upon Formation of Molecular Heterointerfaces. *J. Phys. Chem. C* **2019**, *123*, 12242−12248.

(2) El-Sayed, A.; Borghetti, P.; Goiri, E.; Rogero, C.; Floreano, L.; Lovat, G.; Mowbray, D. J.; Cabellos, J. L.; Wakayama, Y.; Rubio, A.; Ortega, J. E.; de Oteyza, D. G. Understanding Energy-Level Alignment in Donor-Acceptor/Metal Interfaces from Core-Level Shifts. *ACS Nano* **2013**, *7*, 6914−6920.

(3) Akaike, K.; Koch, N.; Heimel, G.; Oehzelt, M. The Impact of Disorder on the Energy Level Alignment at Molecular Donor-Acceptor Interfaces. *Adv. Mater. Interfaces* **2015**, *2*, 1500232.

(4) Goiri, E.; Matena, M.; El-Sayed, A.; Lobo-Checa, J.; Borghetti, P.; Rogero, C.; Detlefs, B.; Duvernay, J.; Ortega, J. E.; de Oteyza, D. G. Self-Assembly of Bicomponent Molecular Monolayers: Adsorption Height Changes and Their Consequences. *Phys. Rev. Lett.* **2014**, *112*, 117602.

(5) Kera, S.; Yamane, H.; Ueno, N. First-Principles Measurements of Charge Mobility in Organic Semiconductors: Valence Hole-Vibration Coupling in Organic Ultrathin Films. *Prog. Surf. Sci.* **2009**, *84*, 135−154.

(6) Ueno, N.; Kera, S. Electron Spectroscopy of Functional Organic Thin Films: Deep Insights into Valence Electronic Structure in Relation to Charge Transport Property. *Prog. Surf. Sci.* **2008**, *83*, 490−557.

(7) Oehzelt, M.; Akaike, K.; Koch, N.; Heimel, G. Energy-Level Alignment at Organic Heterointerfaces. *Sci. Adv.* **2015**, *1*, No. e1501127.

(8) Shi, X.-Q.; Li, Y.; Van Hove, M. A.; Zhang, R.-Q. Interactions between Organics and Metal Surfaces in the Intermediate Regime between Physisorption and Chemisorption. *J. Phys. Chem. C* **2012**, *116*, 23603−23607.

(9) Betti, M. G.; Kanjilal, A.; Mariani, C.; Vázquez, H.; Dappe, Y. J.; Ortega, J.; Flores, F. Barrier Formation at Organic Interfaces in a Cu(100)-Benzenethiolate-Pentacene Heterostructure. *Phys. Rev. Lett.* **2008**, *100*, 027601.

(10) Geim, A. K.; Grigorieva, I. V. Van der Waals Heterostructures. *Nature* **2013**, *499*, 419−425.

(11) Ishii, H.; Sugiyama, K.; Ito, E.; Seki, K. Energy Level Alignment and Interfacial Electronic Structures at Organic/Metal and Organic/Organic Interfaces. *Adv. Mater.* **1999**, *11*, 605−625.

(12) Belova, V.; Beyer, P.; Meister, E.; Linderl, T.; Halbich, M. U.; Gerhard, M.; Schmidt, S.; Zechel, T.; Meisel, T.; Generalov, A. V.; Anselmo, A. S.; Scholz, R.; Konovalov, O.; Gerlach, A.; Koch, M.; Hinderhofer, A.; Opitz, A.; Brutting, W.; Schreiber, F. Evidence for Anisotropic Electronic Coupling of Charge Transfer States in Weakly Interacting Organic Semiconductor Mixtures. *J. Am. Chem. Soc.* **2017**, *139*, 8474−8486.

(13) Hinderhofer, A.; Schreiber, F. Organic-Organic Heterostructures: Concepts and Applications. *ChemPhysChem* **2012**, *13*, 628−643.

(14) Hinderhofer, A.; Frank, C.; Hosokai, T.; Resta, A.; Gerlach, A.; Schreiber, F. Structure and Morphology of Coevaporated Pentacene-Perfluoropentacene Thin Films. *J. Chem. Phys.* **2011**, *134*, 104702.

(15) Thussing, S.; Fernandez, L.; Jakob, P. Thermal Stability and Interlayer Exchange Processes in Heterolayers of TiOPc and PTCDA on Ag(1 1 1). *J. Phys.: Condens. Matter* **2019**, *31*, 134002.

(16) Duhm, S.; Heimel, G.; Salzmann, I.; Glowatzki, H.; Johnson, R. L.; Vollmer, A.; Rabe, J. P.; Koch, N. Orientation-Dependent Ionization Energies and Interface Dipoles in Ordered Molecular Assemblies. *Nat. Mater.* **2008**, *7*, 326−332.

(17) Henneke, C.; Felter, J.; Schwarz, D.; Tautz, F. S.; Kumpf, C. Controlling the Growth of Multiple Ordered Heteromolecular Phases by Utilizing Intermolecular Repulsion. *Nat. Mater.* **2017**, *16*, 628−633.

(18) Wang, Q.; Franco-Cañellas, A.; Ji, P.; Bürker, C.; Wang, R.-B.; Broch, K.; Thakur, P. K.; Lee, T.-L.; Zhang, H.; Gerlach, A.; Chi, L.; Duhm, S.; Schreiber, F. Bilayer Formation vs Molecular Exchange in Organic Heterostructures: Strong Impact of Subtle Changes in Molecular Structure. *J. Phys. Chem. C* **2018**, *122*, 9480−9490.

(19) Stadtmüller, B.; Gruenewald, M.; Peuker, J.; Forker, R.; Fritz, T.; Kumpf, C. Molecular Exchange in a Heteromolecular PTCDA/CuPc Bilayer Film on Ag(111). *J. Phys. Chem. C* **2014**, *118*, 28592−28602.

(20) Thussing, S.; Jakob, P. Thermal Stability and Interlayer Exchange Processes in Heterolayers of CuPc and PTCDA on Ag(111). *J. Phys. Chem. C* **2017**, *121*, 13680−13691.

(21) Bauer, O.; Ikonomov, J.; Schmitz, C. H.; Willenbockel, M.; Soubatch, S.; Tautz, F. S.; Sokolowski, M. Adsorption of 3,4,9,10-Perylenetetracarboxylic Acid Dianhydride on the $Cu_3Au(111)$ Surface Studied by Normal-Incidence X-ray Standing Waves. *J. Phys. Chem. C* **2018**, *122*, 10904−10917.

(22) Blowey, P. J.; Rochford, L. A.; Duncan, D. A.; Warr, D. A.; Lee, T. L.; Woodruff, D. P.; Costantini, G. Probing the Interplay between Geometric and Electronic Structure in a Two-Dimensional K-TCNQ Charge Transfer Network. *Faraday Discuss.* **2017**, *204*, 97−110.

(23) Crispin, X.; Geskin, V.; Crispin, A.; Cornil, J.; Lazzaroni, R.; Salaneck, W. R.; Brédas, J.-L. Characterization of the Interface Dipole at Organic/Metal Interfaces. *J. Am. Chem. Soc.* **2002**, *124*, 8131−8141.

(24) Gerlach, A.; Hosokai, T.; Duhm, S.; Kera, S.; Hofmann, O. T.; Zojer, E.; Zegenhagen, J.; Schreiber, F. Orientational Ordering of Nonplanar Phthalocyanines on Cu(111): Strength and Orientation of the Electric Dipole Moment. *Phys. Rev. Lett.* **2011**, *106*, 156102.

(25) Franco-Cañellas, A.; Wang, Q.; Broch, K.; Duncan, D. A.; Thakur, P. K.; Liu, L.; Kera, S.; Gerlach, A.; Duhm, S.; Schreiber, F. Metal-Organic Interface Functionalization via Acceptor End Groups: PTCDI on Coinage Metals. *Phys. Rev. Mater.* **2017**, *1*, 013001.

(26) Yang, A.; Franco-Cañellas, A.; Sato, M.; Wang, B.; Wang, R.-B.; Koike, H.; Salzmann, I.; Thakur, P. K.; Lee, T.-L.; Liu, L.; Kera, S.; Gerlach, A.; Kanai, K.; Fan, J.; Schreiber, F.; Duhm, S. Nitrogen Substitution Impacts Organic-Metal Interface Energetics. *Phys. Rev. B: Condens. Matter Mater. Phys.* **2016**, *94*, 155426.

(27) Duhm, S.; Gerlach, A.; Salzmann, I.; Broker, B.; Johnson, R. L.; Schreiber, F.; Koch, N. PTCDA on Au(111), Ag(111) and Cu(111): Correlation of Interface Charge Transfer to Bonding Distance. *Org. Electron.* **2008**, *9*, 111−118.

(28) Lu, M. C.; Wang, R. B.; Yang, A.; Duhm, S. Pentacene on Au(1 1 1), Ag(1 1 1) and Cu(1 1 1): From Physisorption to Chemisorption. *J. Phys.: Condens. Matter* **2016**, *28*, 094005.

(29) Gerlach, A.; Schreiber, F.; Sellner, S.; Dosch, H.; Vartanyants, I. A.; Cowie, B. C. C.; Lee, T.-L.; Zegenhagen, J. Adsorption-Induced Distortion of $F_{16}CuPc$ on Cu(111) and Ag(111): An X-ray Standing Wave Study. *Phys. Rev. B: Condens. Matter Mater. Phys.* **2005**, *71*, 205425.

(30) Lo, Y.-Y.; Chang, J.-H.; Hoffmann, G.; Su, W.-B.; Wu, C.-I.; Chang, C.-S. A Comparative Study on the Adsorption Behavior of Pentacene and Perfluoropentacene Molecules on Au(111) Surfaces. *Jpn. J. Appl. Phys.* **2013**, *52*, 101601.

(31) Yang, J. L.; Schumann, S.; Hatton, R. A.; Jones, T. S. Copper Hexadecafluorophthalocyanine ($F_{16}CuPc$) as an Electron Accepting Material in Bilayer Small Molecule Organic Photovoltaic Cells. *Org. Electron.* **2010**, *11* (8), 1399−1402.

(32) Yang, J. L.; Schumann, S.; Jones, T. S. Nanowire-Array Films of Copper Hexadecafluorophthalocyanine ($F_{16}CuPc$) Fabricated by Templated Growth. *J. Mater. Chem.* **2011**, *21* (15), 5812−5816.

(33) de Oteyza, D. G.; El-Sayed, A.; Garcia-Lastra, J. M.; Goiri, E.; Krauss, T. N.; Turak, A.; Barrena, E.; Dosch, H.; Zegenhagen, J.; Rubio, A.; Wakayama, Y.; Ortega, J. E. Copper-Phthalocyanine Based Metal-Organic Interfaces: The Effect of Fluorination, the Substrate, and Its Symmetry. *J. Chem. Phys.* **2010**, *133*, 214703.

(34) Franco-Cañellas, A.; Wang, Q.; Broch, K.; Shen, B.; Gerlach, A.; Bettinger, H. F.; Duhm, S.; Schreiber, F. Resolving Intramolecular-Distortion Changes Induced by the Partial Fluorination of Pentacene Adsorbed on Cu(111). *Phys. Rev. Mater.* **2018**, *2*, 044002.

(35) Heimel, G.; Duhm, S.; Salzmann, I.; Gerlach, A.; Strozecka, A.; Niederhausen, J.; Burker, C.; Hosokai, T.; Fernandez-Torrente, I.; Schulze, G.; Winkler, S.; Wilke, A.; Schlesinger, R.; Frisch, J.; Broker, B.; Vollmer, A.; Detlefs, B.; Pflaum, J.; Kera, S.; Franke, K. J.; Ueno, N.; Pascual, J. I.; Schreiber, F.; Koch, N. Charged and Metallic Molecular Monolayers through Surface-Induced Aromatic Stabilization. *Nat. Chem.* **2013**, *5*, 187−194.

(36) O'Shea, J. N.; Saywell, A.; Magnano, G.; Perdigão, L. M. A.; Satterley, C. J.; Beton, P. H.; Dhanak, V. R. Adsorption of PTCDI on Au(111): Photoemission and Scanning Tunnelling Microscopy. *Surf. Sci.* **2009**, *603*, 3094−3098.

(37) Bouju, X.; Mattioli, C.; Franc, G.; Pujol, A.; Gourdon, A. Bicomponent Supramolecular Architectures at the Vacuum-Solid Interface. *Chem. Rev.* **2017**, *117*, 1407−1444.

(38) Hieulle, J.; Silly, F. Localized Intermolecular Electronic Coupling in Two-Dimensional Self-Assembled 3,4,9,10-Perylenetetracarboxylic Diimide Nanoarchitectures. *J. Mater. Chem. C* **2013**, *1*, 4536−4539.

(39) Kera, S.; Hosokai, T.; Duhm, S. Characteristics of Organic-Metal Interaction: A Perspective from Bonding Distance to Orbital Delocalization. *J. Phys. Soc. Jpn.* **2018**, *87*, 061008.

(40) Klues, M.; Witte, G. Crystalline Packing in Pentacene-Like Organic Semiconductors. *CrystEngComm* **2018**, *20*, 63−74.

(41) Käfer, D.; El Helou, M.; Gemel, C.; Witte, G. Packing of Planar Organic Molecules: Interplay of van der Waals and Electrostatic Interaction. *Cryst. Growth Des.* **2008**, *8*, 3053−3057.

(42) Bürker, C.; Franco-Cañellas, A.; Broch, K.; Lee, T. L.; Gerlach, A.; Schreiber, F. Self-Metalation of 2h-Tetraphenylporphyrin on Cu(111) Studied with XSW: Influence of the Central Metal Atom on the Adsorption Distance. *J. Phys. Chem. C* **2014**, *118*, 13659−13666.

(43) Lee, T.-L.; Duncan, D. A. A Two-Color Beamline for Electron Spectroscopies at Diamond Light Source. *Synchrotron Radiat. News* **2018**, *31*, 16−22.

(44) Franco-Cañellas, A., Duhm, S.; Gerlach, A.; Schreiber, F., Binding and Electronic Level Alignment of π-Conjugated Systems on Metals. *Rep. Prog. Phys.* **2020**, in press. DOI: 10.1088/1361-6633/ab7a42

(45) Hermann, K. E.; Van Hove, M. A. Leedpat. http://www.fhi-berlin.mpg.de/KHsoftware/LEEDpat/, 2014.

(46) Huang, H.; Wong, S. L.; Chen, W.; Wee, A. T. S. LT-STM Studies on Substrate-Dependent Self-Assembly of Small Organic Molecules. *J. Phys. D: Appl. Phys.* **2011**, *44*, 464005.

(47) Mura, M.; Silly, F.; Briggs, G. A. D.; Castell, M. R.; Kantorovich, L. N. H-Bonding Supramolecular Assemblies of PTCDI Molecules on the Au(111) Surface. *J. Phys. Chem. C* **2009**, *113*, 21840−21848.

(48) Wang, C.; Niu, D.; Zhao, Y.; Wang, S.; Qian, C.; Huang, H.; Xie, H.; Gao, Y. Interface Energy-Level Alignment between Black Phosphorus and $F_{16}CuPc$ Molecular Films. *J. Phys. Chem. C* **2019**, *123*, 10443−10450.

(49) Peisert, H.; Knupfer, M.; Schwieger, T.; Fuentes, G. G.; Olligs, D.; Fink, J.; Schmidt, T. Fluorination of Copper Phthalocyanines: Electronic Structure and Interface Properties. *J. Appl. Phys.* **2003**, *93*, 9683−9692.

(50) Evangelista, F.; Carravetta, V.; Stefani, G.; Jansik, B.; Alagia, M.; Stranges, S.; Ruocco, A. Electronic Structure of Copper Phthalocya-

nine: An Experimental and Theoretical Study of Occupied and Unoccupied Levels. *J. Chem. Phys.* **2007**, *126*, 124709.

(51) El-Sayed, A.; Mowbray, D. J.; García-Lastra, J. M.; Rogero, C.; Goiri, E.; Borghetti, P.; Turak, A.; Doyle, B. P.; Dell'Angela, M.; Floreano, L.; Wakayama, Y.; Rubio, A.; Ortega, J. E.; de Oteyza, D. G. Supramolecular Environment-Dependent Electronic Properties of Metal-Organic Interfaces. *J. Phys. Chem. C* **2012**, *116*, 4780−4785.

(52) de Oteyza, D. G.; García-Lastra, J. M.; Corso, M.; Doyle, B. P.; Floreano, L.; Morgante, A.; Wakayama, Y.; Rubio, A.; Ortega, J. E. Customized Electronic Coupling in Self-Assembled Donor-Acceptor Nanostructures. *Adv. Funct. Mater.* **2009**, *19*, 3567−3573.

(53) Henze, S. K. M.; Bauer, O.; Lee, T. L.; Sokolowski, M.; Tautz, F. S. Vertical Bonding Distances of PTCDA on Au(111) and Ag(111): Relation to the Bonding Type. *Surf. Sci.* **2007**, *601*, 1566−1573.

(54) Gerlach, A.; Bürker, C.; Hosokai, T.; Schreiber, F. X-ray Standing Waves and Surfaces X-ray Scattering Studies of Molecule-Metal Interfaces. In *The Molecule-Metal Interface*; Koch, N., Ueno, N., Wee, A. T. S., Eds.; Wiley-VCH: 2013; pp 153−172.

(55) Zegenhagen, J. Surface Structure Determination with X-ray Standing Waves. *Surf. Sci. Rep.* **1993**, *18*, 202−271.

(56) Yamane, H.; Gerlach, A.; Duhm, S.; Tanaka, Y.; Hosokai, T.; Mi, Y. Y.; Zegenhagen, J.; Koch, N.; Seki, K.; Schreiber, F. Site-Specific Geometric and Electronic Relaxations at Organic-Metal Interfaces. *Phys. Rev. Lett.* **2010**, *105*, 046103.

(57) Blowey, P. J.; Maurer, R. J.; Rochford, L. A.; Duncan, D. A.; Kang, J. H.; Warr, D. A.; Ramadan, A. J.; Lee, T. L.; Thakur, P. K.; Costantini, G.; Reuter, K.; Woodruff, D. P. The Structure of VoPc on Cu(111): Does V = O Point up, or Down, or Both? *J. Phys. Chem. C* **2019**, *123*, 8101−8111.

(58) Kera, S.; Fukagawa, H.; Kataoka, T.; Hosoumi, S.; Yamane, H.; Ueno, N. Spectroscopic Evidence of Strong π-πInterorbital Interaction in a Lead-Phthalocyanine Bilayer Film Attributed to the Dimer Nanostructure. *Phys. Rev. B: Condens. Matter Mater. Phys.* **2007**, *75*, 121305.

(59) Liao, M.-S.; Watts, J. D.; Huang, M.-J.; Gorun, S. M.; Kar, T.; Scheiner, S. Effects of Peripheral Substituents on the Electronic Structure and Properties of Unligated and Ligated Metal Phthalocyanines, Metal = Fe, Co, Zn. *J. Chem. Theory Comput.* **2005**, *1* (6), 1201−1210.

(60) Wu, W.; Rochford, L. A.; Felton, S.; Wu, Z.; Yang, J. L.; Heutz, S.; Aeppli, G.; Jones, T. S.; Harrison, N. M.; Fisher, A. J. Magnetic Properties of Copper Hexadecaphthalocyanine (F_{16}CuPc) Thin Films and Powders. *J. Appl. Phys.* **2013**, *113* (1), 013914.

(61) Stadtmüller, B.; Willenbockel, M.; Schröder, S.; Kleimann, C.; Reinisch, E. M.; Ules, T.; Soubatch, S.; Ramsey, M. G.; Tautz, F. S.; Kumpf, C. Modification of the Ptcda-Ag Bond by Forming a Heteromolecular Bilayer Film. *Phys. Rev. B: Condens. Matter Mater. Phys.* **2015**, *91*, 155433.

(62) Wang, Q.; Xin, Q.; Wang, R.-B.; Oehzelt, M.; Ueno, N.; Kera, S.; Duhm, S. Picene Thin Films on Metal Surfaces: Impact of Molecular Shape on Interfacial Coupling. *Phys. Status Solidi RRL* **2017**, *11*, 1700012.

(63) Zojer, E.; Taucher, T. C.; Hofmann, O. T. The Impact of Dipolar Layers on the Electronic Properties of Organic/Inorganic Hybrid Interfaces. *Adv. Mater. Interfaces* **2019**, *6*, 1900581.

(64) Koch, N.; Gerlach, A.; Duhm, S.; Glowatzki, H.; Heimel, G.; Vollmer, A.; Sakamoto, Y.; Suzuki, T.; Zegenhagen, J.; Rabe, J. P.; Schreiber, F. Adsorption-Induced Intramolecular Dipole: Correlating Molecular Conformation and Interface Electronic Structure. *J. Am. Chem. Soc.* **2008**, *130*, 7300−7304.

(65) Toyoda, K.; Hamada, I.; Lee, K.; Yanagisawa, S.; Morikawa, Y. Density Functional Theoretical Study of Pentacene/Noble Metal Interfaces with van der Waals Corrections: Vacuum Level Shifts and Electronic Structures. *J. Chem. Phys.* **2010**, *132*, 134703.

(66) Ferri, N.; Ambrosetti, A.; Tkatchenko, A. Electronic Charge Rearrangement at Metal/Organic Interfaces Induced by Weak van der Waals Interactions. *Phys. Rev. Mater.* **2017**, *1*, 026003.

(67) Bagus, P. S.; Staemmler, V.; Woll, C. Exchangelike Effects for Closed-Shell Adsorbates: Interface Dipole and Work Function. *Phys. Rev. Lett.* **2002**, *89*, 096104.

(68) Koch, N. Organic Electronic Devices and Their Functional Interfaces. *ChemPhysChem* **2007**, *8*, 1438−1455.